Shahrood University of Technology
Iranian Society of Mining Engineering (IRSME)
Journal of Mining and Environment (JME)
journal homepage: www.jme.shahroodut.ac.ir
THOMSON REUTERS
Vol. 10, No. 2, 2019, 373-388.
DOI: 10.22044/jme.2019.7658.1620

# Mechanical activation of phosphate concentrates to enhance dissolution efficiency of rare earth elements from a kinetic viewpoint

H. Shadi Naghadeh[1], M. Abdollahy[1*], A. Khodadadi Darban[1] and P. Pourghahramani[2]

*1. Mining Engineering Department, Tarbiat Modares University, Tehran, Iran*
*2. Mining Engineering Faculty, Sahand University of Technology, Tabriz, Iran*

Received 5 November 2018; received in revised form 31 December 2018; accepted 2 January 2019

**Keywords**

*Esfordi Phosphate Concentrate*

*Rare Earth Elements*

*Mechanical Activation*

*Leaching*

**Abstract**

The Esfordi phosphate concentrate mainly contains fluorapatite, monazite, and xenotime as rare earth element (REE) minerals, accounting for 1.5% of rare earth metals. The monazite and xenotime minerals are refractory and their decomposition is only possible at high temperatures. Thus mechanical activation was used in the present work for this purpose. After 90 minutes of mechanical activation, the X-ray amorphization phase and the maximum BET surface area were increased to 93.4% and 8.4 $m^2/g$, respectively. The Williamson-Hall plot indicated that the crystallite size was decreased and the lattice strain was increased as a function of the milling intensity. A volume-weighted crystallite size of 64 nm and a lattice strain of 0.9% were achieved from the mechanically activated sample for 90 minutes. The leaching efficiency of REEs with 32% nitric acid at 85 °C was increased from 25% for the initial sample to about 95% for the activated samples. The first stage reaction rate constants for La, Nd, and Ce were increased from $8 \times 10^{-7}$, $9 \times 10^{-7}$, and $6 \times 10^{-7}$ for the initial sample to $1.3 \times 10^{-3}$, $9 \times 10^{-4}$, and $7 \times 10^{-4}$ for the mechanically activated samples at 60 °C, respectively. Also the apparent activation energy for La, Nd, and Ce for the initial sample was found to be about 210, 231, and 229 kJ/mol, which were decreased to 120, 91, and 80 kJ/mol, respectively, after 20 minutes of mechanical activation in an argon atmosphere. The results obtained suggested mechanical activation as an appropriate pre-treatment method for dissolution of REEs from phosphate concentrates containing refractory REE minerals at a lower cost and a higher recovery rate.

## 1. Introduction

Rare earth elements (REEs) contain 17 metal elements in the periodic table, of which 15 elements are in the lanthanide group and the two others are scandium and yttrium. These elements are similar in many aspects owing to their geological origin but they are different in terms of dispersion and concentration [1].

Because of the industrial development in the use of REEs, the Chinese government reduced its annual export in 2017 to about 39,800 metric tons of rare earth oxides, while the global demand in 2017 was 130,000 metric tons [2]. This scarcity of resources has led to the development of many new projects for the extraction and processing of REEs, each having its own mining and processing challenges. One of these new projects is the Esfordi Complex located in the center of Iran in the Yazd Province. The Esfordi flotation concentrates contain 1.2-1.5% of total REEs often found in the fluorapatite, monazite, and xenotime minerals [3, 4]. Hydrometallurgical extraction of REEs from the mentioned minerals is technically a difficult process with severe reaction conditions [4]. Given the remarkable grade of REEs in the Esfordi phosphate concentrate as a secondary source of REEs, the introduction of new methods for the hydrometallurgical treatment of REEs is of prime importance.

*Corresponding author: minmabd@modares.ac.ir (M. Abdollahy).*

Due to the significant structural changes during mechanical activation, it could be a promising method for improving the reactivity of the refractory minerals containing REEs. Mechanical activation is a part of the mechano-chemical knowledge with many applications. Mechanical activation increases the material reaction speed. In other words, their dissolution temperature was decreased to lower than that in the conventional processes. Changes in the structural characteristics of materials caused by mechanical activation improve the reactivity of the activated materials [5]. Many of these advantages are linked to changes in the structure of materials. Previous studies have shown an increase in the amorphization degree and micro-strain and a decrease in the crystallite size; the polymorphic phase deformation and particle deformation can cause structural changes in the activated materials [6]. Some researchers have used mechanical activation to improve the hydrometallurgical processing of refractory minerals. It has been indicated that mechanical activation can increase the solubility of minerals because of the structural irregularities and the formation of new surfaces [7, 8]. Mechanical activation has been used to increase the leaching speed of pyrrhotite, and its effect on the kinetics of pyrrhotite leaching with the iron(III) chloride–hydrochloric acid reagent has been studied. It has been concluded that mechanical activation not only extremely decreases the apparent activation energy but also notably improves the leaching rate [9]. The mechanical activation pre-treatment method has been utilized for inducing physico-chemical changes on the lateritic nickel ore structure. The fast kinetics of leaching and low acid consumption have been reported to be the main advantages of mechanical activation as a pre-treatment method [10]. Mechanical activation was previously used for changing the structural properties of the boron concentrate. Furthermore, the activated concentrate was leached. Also the effects of surface free energy and specific surface area on the leaching speed have been investigated. The results obtained showed that both surface chemical reactions and penetration in the product layer controlled the leaching of mechanically activated concentrate but in the case of non-activated samples, the surface chemical reaction was able to control the leaching process. It has been proven that increasing the mechanical activation time reduces the apparent activation energy and the leaching reaction order [11]. The researchers have used calcium chloride and calcium oxide as the mechano-chemical activation agents for the decomposition of monazite. Using this method has decomposed nearly 95% of monazite [12]. For a complete decomposition of monazite and production of REE hydroxides, the mechano-chemical activation pre-treatment method in the presence of sodium hydroxide has been used [13]. Mechano-chemical activation in the presence of sodium hydroxide has also been used to extract REEs from bastnaesite. The results obtained showed that using mechano-chemical activation led to the production of REE hydroxides and sodium-rich compounds [14]. In the mentioned research work, about 90% of the produced REE hydroxides was dissolved in the presence of dilute sulfuric acid and conventional leaching conditions [14, 15].

Mechanical activation has also been used for the recovery of REEs from fluorescent lamps. The results obtained showed that the activation energy of REE leaching was reduced and the dissolution yields was increased by about 90% using mechanical activation [16]. It has been shown that mechanical activation causes structural defects and breaking of crystalline network in waste trichromatic phosphors separated from e-waste, which plays a major role in increasing the solubility of REEs. Reducing crystallinity has the greatest effect on increasing the solubility of REEs [17]. The use of mechanical activation increased the solubility of REEs in fluorescent lamps from 0.9% to 81% at room temperature. The shrinking core model has been employed as a suitable kinetic model for dissolution, and the amount of the apparent dissolution activation energy has been reduced from 68 to 1.4 kJ/mol. These changes were explained by reducing the particle size, increasing the surface area, and changing the crystalline structure [18].

In the present research work, the planetary ball mill was used to activate the Iranian apatite concentrate for the dissolution of REE metals. In addition, the structural changes of the mechanically activated phosphate concentrate were studied using the line profile analysis of X-ray diffraction (XRD) patterns. Finally, the influence of mechanical activation on the leachability of phosphate concentrate during the hydrometallurgical treatment was considered, which had not been mentioned before.

## 2. Materials and methods

### 2.1. Materials

Highly pure apatite concentrate was kindly donated by Esfordi Complex located in the center

of Iran in the Yazd Province. A 250-kg concentrate with $d_{80}$ = 54 µm containing 1.2% total REE and 16.31% phosphorus was initially homogenized. The chemical composition of the initial sample is shown in Table 1. The representative sub-samples were used for identification, mechanical activation, and leaching. As it can be seen in Table 1, the concentrate contained 37.13% Ca, 16.31% P, 2.91% Fe, and a total of 1.2% REEs. Based on the polish section studies using an optical microscope, fluorapatite was the major phosphorus and calcium mineral in the phosphate concentrate. Fluorapatite accounted for 89% of the concentrate (Table 2).

The EMPA analysis was used for a detailed identification of refractory minerals in the phosphate concentrate. It was shown that the size of the rare earth mineral particles was between 1 and 20 µm but in some cases, their size exceeded 50 µm, usually the liberated particles. In general, d80 of the REE minerals (monazite and xenotime) could be considered to be about 20 µm. As shown in Figure 1, the rare earth minerals are often found as an inclusion in apatite (more than 90%), and rarely inside hematite and in the border between apatite and quartz.

**Table 1. Chemical composition of the phosphate concentrate [3].**

| Major elements | | Minor elements | | Rare earths | |
|---|---|---|---|---|---|
| **Element** | **Mass percentage (%)** | **Element** | **ppm (mg/kg)** | **Element** | **ppm (mg/kg)** |
| Ca | 37.13 | Si | 7500 | Ce | 5608 |
| P | 16.31 | Mg | 2055 | Nd | 2227 |
| Fe | 2.91 | Na | 1476 | La | 1959 |
| F | 3.00 | Al | 1127 | Y | 679.7 |
| Cl | 0.33 | S | 692 | Pr | 614.1 |
| | | Sr | 333.8 | Sm | 342.9 |
| | | Ti | 213 | Dy | 154.1 |
| | | K | 220 | Er | 129.8 |
| | | V | 123 | Eu | 29.4 |
| | | Mn | 88 | Lu | 4.3 |
| | | Th | 82.5 | Tb | 42.6 |
| | | U | 4.6 | Yb | 31.7 |
| | | | | Gd | 188.1 |

**Table 2. Mineralogical analysis of the Esfordi phosphate concentrate [3].**

| **Mineral** | **Fluorapatite $(Ca,REE)_5(PO_4)_3F$** | **Monazite $REEPO_4$** | **Xenotime $YPO_4$** | **Maghemite $Fe_2O_3$** | **Calcite-Dolomite $CaCO_3$-$CaMgCO_3$** | **Quartz $SiO_2$** | **Other silicates** |
|---|---|---|---|---|---|---|---|
| Percentage (%) | 88.7 | 1.2 | 0.2 | 4.8 | 2.3 | 0.7 | 2.1 |

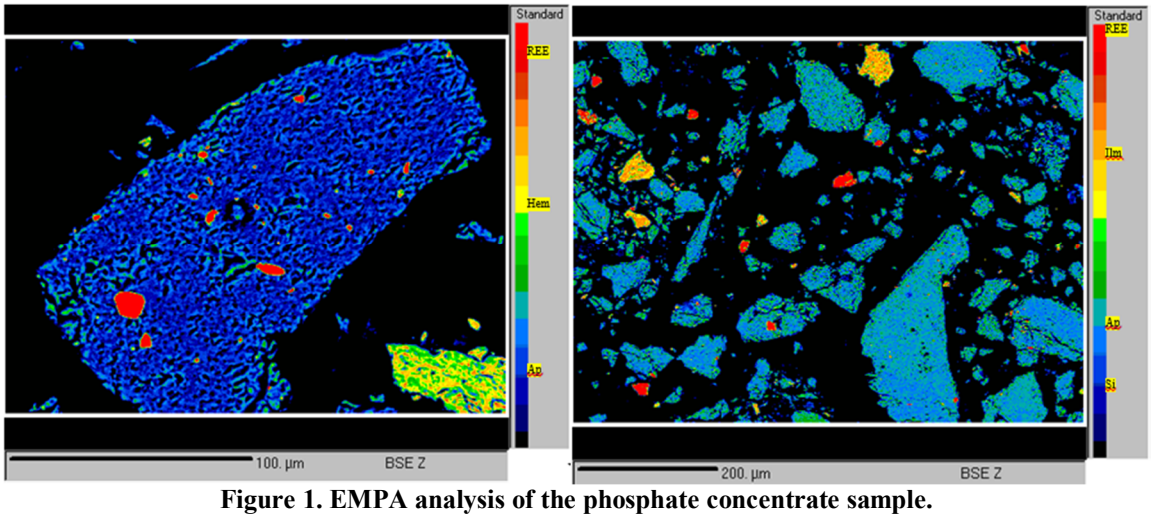


**Figure 1. EMPA analysis of the phosphate concentrate sample.**

### 2.2. Mechanical activation

The phosphate concentrate samples were mechanically activated by a planetary ball mill (Pulverisette 6, FRITSCH, Germany) at 500 rpm in the dry mode, and in an argon atmosphere to prohibit any possible reaction. Stainless steel balls (diameters of 9.4 and 20 mm) and a steel pot were used for milling with a mass ratio of 20:1 (balls to powder ratio). After mechanical activation of the phosphate concentrate samples for 20, 60, and 90 min, the powders were stored in a freezer under completely isolated conditions. The X-ray diffraction (XRD) patterns obtained showed that neither main phase changes nor oxidation occurred because of mechanical activation.

### 2.3. Structural analysis of activated samples

#### 2.3.1. XRD analysis

XRD techniques are usually used for a semi-quantitative phase analysis and to identify unknown crystalline materials. It is currently the most favored technique for the quantitative analysis of the micro-structure of mechanically activated minerals. The micro-structure measurements are based upon the XRD profile physical broadening. The structural plastic deformation of mechanically activated minerals increases the broadening of XRD profiles. In addition, peak broadening increases continuously with an increase in the degree of deformation, simultaneously. In practice, instrumental and sample contributions are two main sources of broadening. After removing the instrumental effects, the broadened profile of mechanically activated minerals exhibited structural defects in the crystallite such as the crystallite size and micro-strain [19]. Accordingly, the identification of structural deformation resulting from the mechanical activation of Esfordi phosphate concentrate is necessary to evaluate the effectiveness of mechanical activation. XRD analysis was used to test the phosphate concentrate, milled (activated), and standard LaB6 SRM-660a samples. The XRD pattern for the initial phosphate concentrate is shown in Figure 2. The standard XRD was used to correct the instrumental effects (Figure 3) by eliminating them from the broadened peaks. The XRD tests were performed by a Bruker Axs D8 using Co Kα radiation (λ = 1.791 Å) at 50 kV and 250 mA (18° to 50°). The scanning conditions of all samples were at the step size of 0.01 and counting time of 5 s per step.

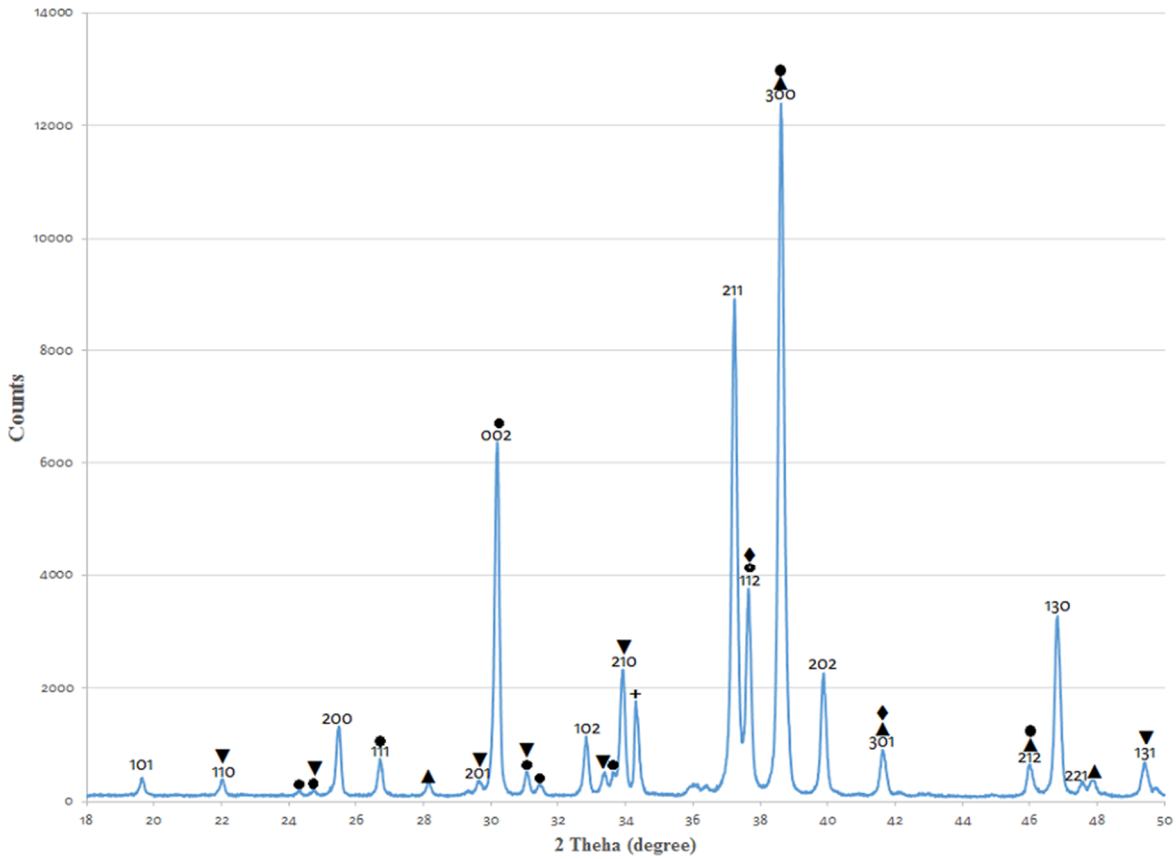


**Figure 2. XRD pattern for the initial phosphate concentrate.**

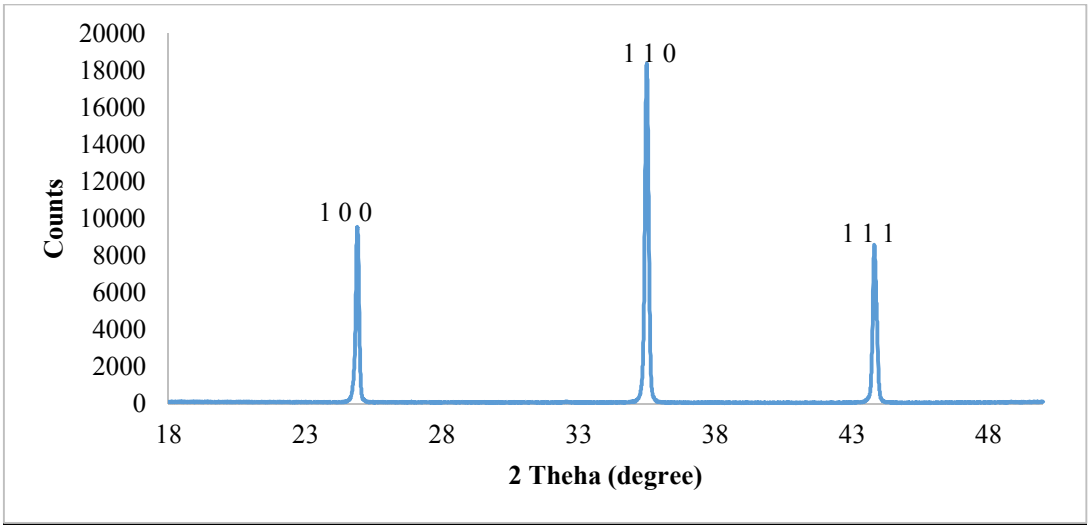


**Figure 3. XRD pattern for the standard LaB6 (SR M660a).**

### 2.3.2. Process of pattern fitting on peaks obtained from XRD analysis

XRD analysis provides various information about the atomic structure of minerals and crystalline materials. As seen in Figure 4, the Winfit software was used for fitting the measured XRD profiles to a linear combination of Cauchy and Gaussian function (the Pseudo-Voigt line shape function). The intensity of kα2 assumes that half part of the kα1 and kα2 components should be subtracted from the XRD patterns. Also smoothing of the XRD profiles was prevented during the fitting. The position and intensity of the XRD peaks and the peak breadth were the initial necessary input information to extract the structural data such as micro-strain, crystallite size, and amorphous phase formation. The accuracy of the micro-structure checking methods is a function of the input data verity including the location of diffracted peak, intensity of diffracted peaks (I), full width at half maximum (FWHM), and integral broadening of the peaks [20].

The fitting process should be implicated for all XRD profiles in order to extract exactly the mentioned parameters. For this purpose, the peaks (101), (110), (200), (111), (002), (102), (210), (211), (112), (300), (202), (301), (212), (130), and (131) were selected. Calculation of the structural parameters from the overlapping peaks requires a separation process. Although a complete separation of the overlapping peaks was not possible, to increase the accuracy of results, the overlapping peaks were roughly separated using the Winfit software at the fitting pattern stage. The XRD profile of the standard sample (LaB6 SMR-660a) was used in the fitting pattern stage.

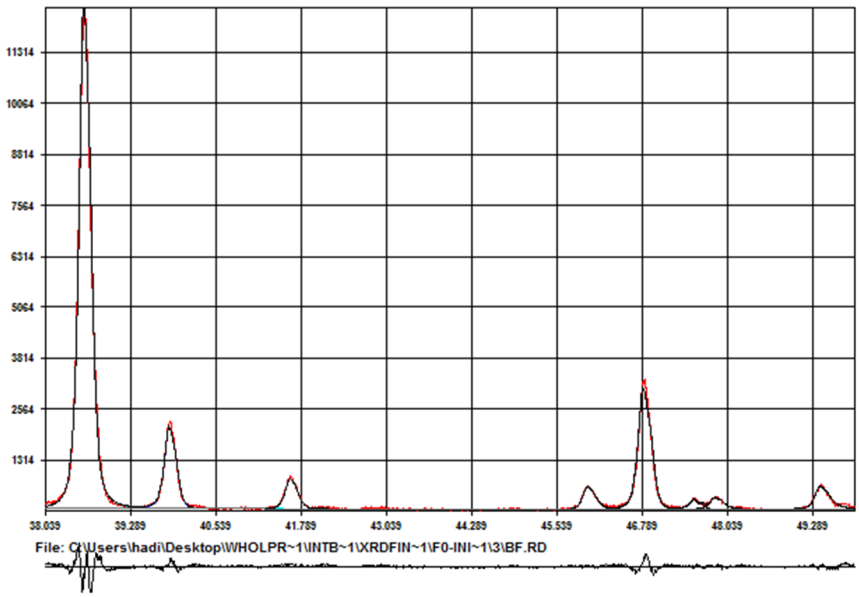


**Figure 4. A typical profile fitting plot of initial phosphate concentrate conducted by Pseudo-Voigt function.**

### 2.3.3. Characterization of micro-structures

An ideal XRD peak should be sharp and non-broadened [21]. The linear breadth of XRD profiles was generated by the combination of three effective sources including the contribution of the XRD instrument, crystallite size, and micro-strain. The effects of the XRD instrument were eliminated using a standard powder of lanthanum hexaboride. Then the effects of crystallite size and micro-strain were differentiated and calculated using the Williamson-Hall plots by the following equations:

$$\beta_f = \frac{\beta_h^2 - \beta_g^2}{\beta_h} \quad (1)$$

$$B = \frac{\beta_f \cos\theta}{\lambda} \quad (2)$$

$$D = \frac{2\sin\theta}{\lambda} \quad (3)$$

$$B^2 = \frac{1}{D_v^2} + 4\varepsilon^2 D^2 \quad (4)$$

where $\beta_f$ refers to the peak integral broadening related to the crystallite size and micro-strain effect, $\beta_h$ and $\beta_g$ represent the instrumental and observed integral broadening, respectively, $\theta$ and $\lambda$ are the peak position and X-ray wavelength, respectively, $D_V$ illustrates the volume weighted crystallite size, and B and D refer to the overall integral broadening and the length of the XRD vector for the reflection intended, respectively [22]. By plotting $B^2$ in terms of $D^2$, the crystallite size and micro-strain can be calculated from the intercept and the gradient of the diagram, respectively. The crystallite size obtained by the Williamson-Hull plot showed the crystallite size based on the volumetric mass.

### 2.3.4. BET and particle size analysis

The BET surface area analysis was performed using a standard BET analyzer (Quantachrome Instruments CHEMBET-3000, USA). The granulometric size and surface area of the particles were also measured using a particle size analyzer (ANALYSETTE 22 Nano Tec plus, FRITSCH, Germany).

### 2.4. Leaching experiments and kinetics modeling

The initial phosphate concentrates and the mechanically activated samples were leached in a nitric acid medium. In all the leaching experiments, highly purified laboratory-graded distilled water and nitric acid were used. A 1-L insulated glass reactor immersed in a water bath with automatic water temperature control was used to carry out the leaching experiments. When the temperature reached the pre-determined value (85 °C), the powder was added to the leaching solution. The pH, temperature, and concentration of the elements in the leaching solution were measured regularly. Having completed the leaching process (2 h), the pulp was filtered and the residual solid was washed three times with a 1% nitric acid solution. The leaching experiments were carried out in nitric acid with a solid weight of 5% and an acid concentration of 32%. The rotation speed of the stirrer was kept at 1000 rpm for all tests. REE and phosphate were measured by an ICP-MS and a spectrophotometer, respectively.

The REE leaching kinetics of the activated and non-activated phosphate concentrates were investigated at 60, 70, and 85 °C. The initial phosphate concentrate and the mechanically activated sample (with 20 mm balls for 20 min in an argon atmosphere) were used to study the kinetics and activation energy. Shrinking core with single stage reacting models (diffusion and chemical control) was used for the kinetic modeling of the leaching experiment but the results obtained were not suitable. Therefore, a two-stage model (combination of diffusion and chemical control) was applied for modeling the REE leaching of the activated and non-activated samples. The leaching results were in good agreement with those for the selected model. After determining the appropriate kinetic model, the reaction rate constant was determined and used to draw the Arrhenius curve. The apparent activation energy of the activated and non-activated samples was calculated by the Arrhenius relationship.

## 3. Results and discussion

In this work, the effect of mechanical activation on the structural changes of the fluorapatite, kinetics, and activation energy of leaching of REEs from the phosphate concentrate was investigated at conventional leaching conditions. In the previous studies, the leaching of REEs from the phosphate concentrate has been investigated using a highly concentrated sulfuric acid at a high temperature, which in addition to a high corrosion and a high environmental pollution, requires a lot of energy. Investigations have shown that the leaching rate of REEs from the phosphate concentrate with sulfuric acid at conventional leaching conditions is very low, and gypsum precipitation is formed [3, 4]. The results of this

work showed that the use of mechanical activation induced structural changes in fluorapatite, which would reduce the activation energy and increase the reaction rate constant of REEs leaching from the phosphate concentrate at low temperatures. Also the use of nitric acid as a substitute for sulfuric acid prevented the formation of gypsum precipitation at low temperatures.

### 3.1. Specific surface area

Table 3 shows the particle size variations after mechanical activation in an argon atmosphere as a function of time and ball diameter. The average granulometric particle size of the phosphate concentrate (before activation) was about 16.3 µm, which was decreased sharply to 4.6 and 9.2 µm after 20 and 60 min of mechanical activation using 9.4 and 20 mm balls, respectively. Using 9.4 mm balls for mechanical activation, the particle size was increased from 4.6 at 20 min to 7.1 and 7.6 µm after 60 and 90 min of mechanical activation, respectively. In the case of 20 mm balls, the particle size was increased from 9.2 at 60 min to 10.5 µm after 90 min. An increase in the particle size through a resumption of mechanical activation confirmed an occurrence of particle agglomeration. It is worth mentioning that before agglomeration, increasing the particle size continued but more steeply.

The changes in the specific surface area during mechanical activation in the argon atmosphere are shown in Figure 5 as a function of the milling time. In the mechanical activation with 9.4 mm balls, the granulometric surface area of the phosphate concentrate sample was increased from 1.14 to 2.61 $m^2/g$ after 20 min but decreased to 1.79 $m^2/g$ after 60 min activation. Using 20 mm balls for mechanical activation, the granulometric surface area was increased from 1.14 to 1.94 and 2.09 $m^2/g$ after 20 and 60 min of mechanical activation, respectively. Then it was dropped to 1.84 $m^2/g$ after 90 min. By increasing the milling time, a decrease in the particle size and an increase in the specific surface area were expected but the reverse results were achieved because of the agglomeration of the activated particles.

Finally, the specific surface area of 4.04 $m^2/g$ (obtained from the BET analysis) in the initial phosphate concentrate sample was increased to 7.34, 8.1, and 8.4 $m^2/g$ using 9.4 mm balls for 20, 60, and 90 min, respectively. Using 20 mm balls, it was increased to 5.91, 6.72, and 6.51 $m^2/g$ for 20, 60, and 90 min, respectively. While the specific surface area arising from laser diffraction showed the beginning of the agglomeration process, the specific surface area of the BET analysis showed that the agglomeration phenomenon could fill the accumulated particle pores. Therefore, the pores were not accessible for the nitrogen gas during the BET analysis. The changing speed of the specific surface area of the BET analysis after agglomeration was almost slow, unlike the initial changing rate.

The mean size of particles ($d_{av}$) was computed using the specific surface area resulting from the BET analysis and the specific weight of the powder (Equation 5):

$$d_{av} = \frac{6}{\sigma s} \quad (5)$$

where σ and S represent the specific weight ($g/cm^3$) and the specific surface area of BET ($m^2/g$), respectively, and $d_{av}$ represents the diameter of the spherical particles in micron. The BET particle size (Table 3) was decreased from 0.48 to 0.26, 0.24, and 0.23 µm using 9.4 mm balls after mechanical activation for 20, 60, and 90 min, respectively. It was decreased to 0.33, 0.29, and 0.3 µm for the mechanically activated phosphate concentrate using 20 mm balls for 20, 60, and 90 min, respectively. It could be concluded that the use of balls with a higher surface area (9.4 mm diameter) for mechanical activation further reduced the particle size and thus increased the specific surface area of the activated sample.

**Table 3. Variation in particle size at different mechanical activation times.**

| Mechanical activation time (min) | 0 | 20 | 60 | 90 | 20 | 60 | 90 |
|---|---|---|---|---|---|---|---|
| Ball diameter (mm) | - | 9.4 | 9.4 | 9.4 | 20 | 20 | 20 |
| Granulometric particle size (µm) | 16.3 | 4.6 | 7.1 | 7.6 | 9.6 | 9.2 | 10.5 |
| BET particle size (µm) | 0.38 | 0.28 | 0.30 | 0.29 | 0.29 | 0.28 | 0.30 |

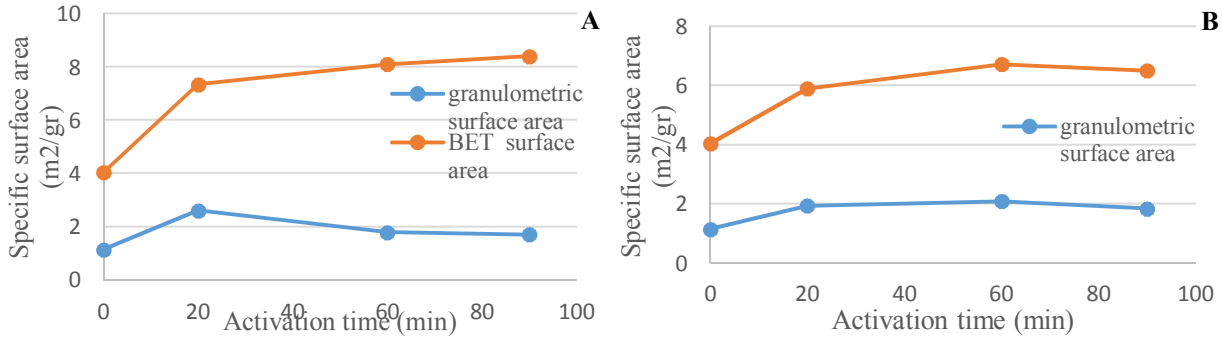


**Figure 5. Effect of activation time on the specific surface area of particles with A) 9.4 mm balls and B) 20 mm balls.**

### 3.2. XRD analysis

The XRD profiles of the non-activated and activated samples showed that all peaks were consistent with the standard XRD profile for fluorapatite with the hexagonal crystallization system and the p63/m space group (JCPDS No. 1-083-0557). Equations (6) and (7) indicate the Bragg equations and the lattice parameter of hexagonal fluorapatite, respectively. Accordingly, transferring the position of diffraction peaks to lower angles indicated that mechanical activation increased the unit cell sizes [18]:

$$N\lambda = 2d\sin\theta \quad (6)$$

$$\frac{1}{d^2} = \frac{4}{3}\left(\frac{h^2 + hk + k^2}{a^2}\right) + \frac{l^2}{c^2} \quad (7)$$

where d is the interplanar spacing, known as the order of reflection (n = 1, 2, 3, …), and h, k, and l are the Miller indices of the diffraction planes.

As shown in Figure 6, the XRD profiles of the non-activated and mechanically activated samples showed that an increase in the milling time resulted in an increase in the breadth of the reflected peaks besides a decrease in the intensity but the impact of small balls (9.4 mm) was more intensive than that of big balls (20 mm). Intensity decrease of the peaks could be attributed to the amorphous phase production during high energy ball milling. Amorphization is a strong distortion of the periodicity of lattice structure as well as the components of the mineral lattice [23]. Materials with a fully crystalline structure have a long-range order compared to the amorphous materials, in which the atoms have a short-range order [23]. Therefore, as already mentioned, the degree of amorphization could be associated with the weakening of bonds between the atoms in minerals [24]. The amorphization degree of activated samples (A) was computed using 10 peaks with the highest intensity based on Equation (8).

$$A(\%) = 100 - \left(\frac{U_0}{I_0} * \frac{I_x}{U_x} * 100\right) \quad (8)$$

where $U_0$ and $U_x$ represent the background of the non-activated and activated powders, respectively, and $I_0$ and $I_x$ represent the integral intensity of the diffraction lines of the non-activated and activated samples, respectively. As shown in Figure 7, the degree of amorphization increased sharply in the first stage of milling and then reached a maximum value of 93.38% and 86.64% after 90 min of mechanical activation with 9.4 and 20 mm balls, respectively. In the case of using smaller balls, the degree of amorphization was larger than that using bigger balls. The relatively high degree of amorphization of mechanically activated samples (over 85%), even in moderate activation conditions, indicates the non-refractory nature of fluorapatite as the main mineral of the concentrate during the pre-treatment of mechanical activation.

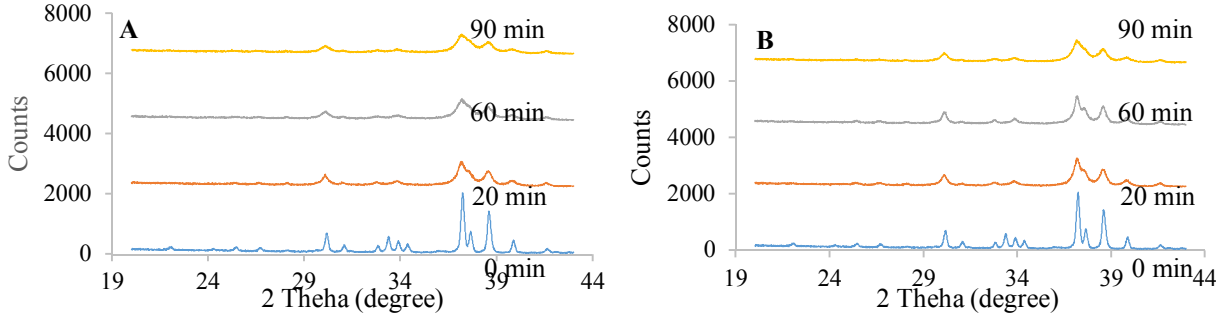


**Figure 6. XRD profiles of the non-activated and mechanically activated powders for different activation times: A) 9.4 mm balls, and B) 20 mm balls.**

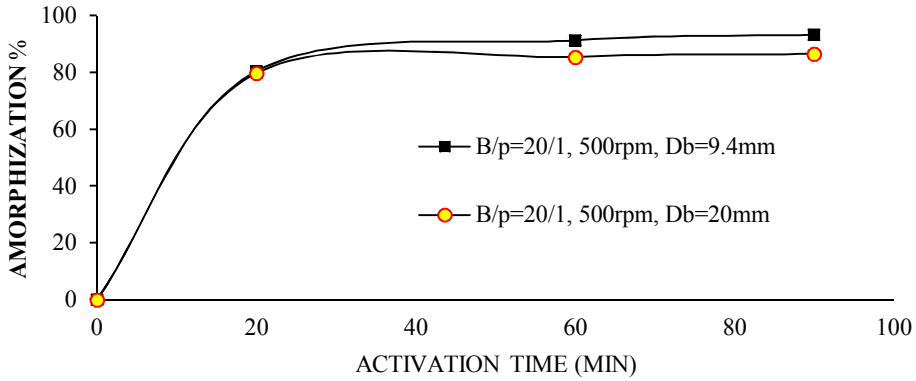


**Figure 7. Changes in the amorphization degree as a result of high-intensity ball milling of the phosphate concentrate.**

### 3.3. Micro-structure characterization

The micro-strain could be attributed to a change in the position of the atoms and the distance between the atomic plates in the mineral structure [25]. Using the Williamson-Hall method, a line profile analysis was used to investigate the changes in the micro-structure of the phosphate concentrates during mechanical activation. The Williamson-Hall plots were used to extract the crystallite size and micro-strain data from the integral breadth of peaks. The results of the Williamson-Hall plots are shown in Table 4. An increase in the activation time decreased the crystallite size, while the inverse occurred for the micro-strain. The results obtained were in good agreement with those of the previous studies [26, 27].

The Williamson-Hall plots were drawn using Equation (4). The curves were obtained from all diffracted peaks using the regression method. The volume-weighted crystallite size and the micro-strain were obtained from the intercept and slope of the Williamson-Hall curves, respectively (Figure 8). If the points were placed on a nearly horizontal line, the effect of the micro-strain component on the broadening of the peak would be negligible (first regression line). On the other hand, as shown in the Williamson-Hall curves, increasing the micro-strain caused an increase in the slope of the regression line either (Figure 8). As noted in the previous studies, when plotting the Williamson-Hall curves, if all points in a regression line do not appear in a straight line, the crystallite size gets slightly different in various direction due to the hexagonal crystal structure of fluorapatite particles [20].

The results of the Williamson-Hall method showed that mechanical activation reduced the crystallite size and increased the micro-strain. The extent of changes was remarkable by the smaller balls (9.4 mm) for activation compared to the bigger balls (20 mm). In the first 20 min of mechanical activation, there was a severe change in the slope of crystallite size decrease and micro-strain increase. The continuation of mechanical activation from 20 to 90 min decreased the variation slopes of the crystallite size and the micro-strain. The main reason could be because of plastic changes or crushing of the particles during mechanical activation. By increasing the intensity of mechanical activation and also the accumulation of particle surface energy, the particles exceeded the rupture limit, and the accumulated energy was, finally, released.

**Table 4. The results of micro-strain and crystallite size calculation of non-activated and activated fluorapatite powders using the Williamson-Hall method.**

| Ball diameter (mm) | Milling time (min) | Crystallite size (nm) | Micro-strain (%) |
|---|---|---|---|
| | 0 | 225 | 0.09 |
| 9.4 | 20 | 90 | 0. 66 |
| 9.4 | 60 | 69.23 | 0. 89 |
| 9.4 | 90 | 64.29 | 0.9 |
| 20 | 20 | 112.5 | 0.51 |
| 20 | 60 | 100 | 0.53 |
| 20 | 90 | 90 | 0.55 |

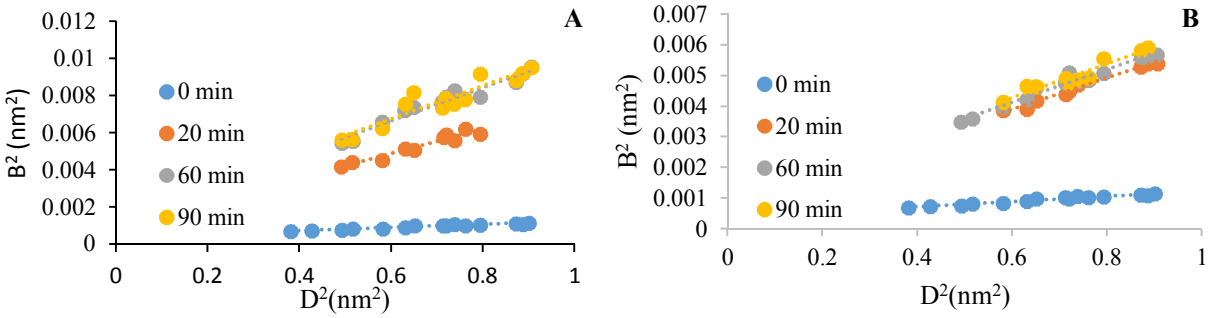


**Figure 8. The Williamson-Hall curves of non-activated and activated phosphate concentrates: A) 9.4 mm balls and B) 20 mm balls.**

### 3.4. Leaching experiments

The structural changes during mechanical activation could have an important role in improving the reactivity of refractory minerals containing REEs. The study of structural changes showed that high-intensity milling had a direct impact on the crystallinity, crystallite size, and amount of micro-strain in the mechanically activated samples. The crystallite size of mechanically activated minerals was small, so there were many intergranular boundaries with more atoms ready to react [28]. Furthermore, the high degree of amorphization suggests that the atomic bonds between the constituent elements of the minerals are diminished and their reactivity increases [24]. Finally, the distance between the atomic planes in the structure of mineral changed due to the applied stress. Therefore, the micro-strain could be related to the changes in the position of the atoms [29] and its improvement could increase the reactivity of mechanically activated minerals [30]. In the previous sections, it was concluded that the mechanical activation increased the structural changes with different effects on the reactivity of phosphate concentrate, especially in the case of amorphization degree, micro-strain increase, and crystallite size reduction.

In the mechanical activation pre-treatment, an increase in amorphization consumed much portion of the applied energy in comparison to the crystallite size and micro-strain changes [20]. In the mechanical activation of phosphate concentrate, the portion of crystallite size reduction in the consumed energy could be neglected because of its close value. The amorphization degree was the most important parameter that enhanced the leachability of the mechanically activated phosphate concentrate [20].

Therefore, efforts were made to increase the effects of micro-structure distortion on the reactivity of phosphate concentrate in practical applications such as leaching. As mentioned above, a high temperature and concentrated acids were required to decompose the rare earth refractory minerals. In the present experiment, mechanical activation could change the structure of refractory minerals; therefore, the extraction of metals was increased in the subsequent hydrometallurgical reactions of minerals.

The results of leaching experiments showed that changes in the structure of minerals existing in the Esfordi phosphate concentrate could improve the reactivity of rare earth minerals. For this purpose, the leaching experiments were performed on the initial and mechanically activated phosphate concentrates at 85 °C using 32% nitric acid. According to Table 5, the maximum leaching efficiency of REEs was obtained for the samples mechanically activated for 20 and 60 min using 20 and 9.4 mm balls, respectively, in which about 95% of the total REEs could be extracted. The efficiency of REE dissolution for the non-activated phosphate concentrate was about 25% in the same leaching conditions. Earlier studies have shown that less than 30% of REEs are in the fluorapatite structure and more than 70% of them are in the form of monazite and xenotime minerals. To dissolve them, temperatures above 200 °C are required. The extraction of REEs from the phosphate concentrate in normal leaching conditions with 98% sulfuric acid is less than 28%, which is consistent with the results of this work [3, 4]. The results obtained showed that mechanical activation could effectively improve the leaching of REE minerals.

The leaching results suggested that mechanical activation directly destroyed the interatomic bonds of refractory minerals of REEs. Therefore, the reactivity of mechanically activated phosphate concentrate increased. To show this, the apparent activation energy and the kinetics of the initial and activated phosphate concentrates leaching were calculated.

**Table 5. Results of phosphate concentrate leaching and mechanically activated phosphate concentrate (leaching conditions: 85 °C, 32% nitric acid, and 120 min).**

| | | | | | | | | |
|---|---|---|---|---|---|---|---|---|
| **Mechanical activation parameters** | **Mechanical activation time** | 0 | 20 | 60 | 90 | 20 | 60 | 90 |
| | **Ball/powder** | - | 20 | 20 | 20 | 20 | 20 | 20 |
| | **Ball diameter (mm)** | - | 9.4 | 9.4 | 9.4 | 20 | 20 | 20 |
| | **Mill rotation speed (rpm)** | - | 500 | 500 | 500 | 500 | 500 | 500 |
| **REE extraction (%)** | **Ce** | 25.1 | 78.1 | 90.2 | 89.9 | 88.4 | 87.1 | 76.2 |
| | **La** | 27.5 | 84.8 | 98.9 | 98.2 | 96.2 | 94.7 | 87.2 |
| | **Nd** | 24.3 | 75.6 | 88.4 | 87.9 | 87.2 | 85.8 | 79.9 |

### 3.4.1. Leaching kinetics of activated and initial phosphate concentrates

The leaching process of lanthanum, neodymium, and cerium was a solid-liquid multi-phase reaction, in which the leaching reaction occurred at a two-phase boundary. The typical model in most of the two-phase solid-liquid reactions was a shrinking core model. Two types of models for single-stage reactions (Equations 9 and 10) were fitted on the results obtained from the REEs of an initial sample and the activated phosphate concentrate leaching. The results obtained showed that none of the mentioned models was appropriate:

$$1-(1-X_B)^{1/3}=K_c t \quad (9)$$

$$1-(2/3X_B)-(1-X_B)^{2/3}=K_D t \quad (10)$$

where $X_B$, $K_C$, $K_D$, and t refer to the reacted portion, chemical and diffusion reaction rate constant, and time, respectively [31, 32, and 33].

The remaining REE concentration (in the leaching residue) curves (Figures 9 and 10) shows that the reaction rate was high in the first 10 min, which was reduced up to 120 min. It seems that the leaching process of REE of the phosphate concentrate has two different behaviors, before and after 10 min. Therefore, a two-stage model was used to fit on the REE leaching results of the non-activated and activated phosphate concentrates (Equations 11 and 12) [34].

Then $K_1$ and $K_2$ were calculated using the following equations:

$$A \rightarrow B,$$

$$-r_A=\frac{dC_A}{dt}=\frac{K_1 C_A}{1+K_2 C_A} \quad (11)$$

$$\frac{Ln(C_{A_0}/C_A)}{C_{A_0}-C_A}=K_2+\frac{K_1 t}{C_{A_0}-C_A} \quad (12)$$

where A and B are the reactants and products, $r_A$ is the reaction rate, $C_{A0}$, $C_A$, $K_1$, $K_2$, and t are the metal concentration in the initial sample, leached sample, first stage reaction rate constant, second stage reaction rate constant, and time, respectively. By putting $\frac{Ln(C_{A_0}-C_A)}{C_{A_0}-C_A}$ in terms of $\frac{t}{C_{A_0}-C_A}$, the first and second stage reaction rate constants ($K_1$ and $K_2$) could be calculated from the gradient and the intercept of the curves, respectively. As shown in Figures 11 to 12, the reaction rate constant values for leaching the lanthanum, neodymium, and cerium elements of the initial and activated samples were calculated using Equation (12) [34].

The results obtained showed that Equation 12 was an appropriate model for the leaching kinetics of REEs in the activated and non-activated phosphate concentrates. In addition, the leaching rate was sensitive to temperature. Also mechanical activation caused an intense increase in the reaction rate. For instance, the K1 and K2 of lanthanum leaching at 85 °C was increased from 0.0002 and 0.1132 for an initial sample to 0.026 and 0.1366 for the mechanically activated sample in the argon atmosphere for 20 min with 20 mm balls, respectively. It seems that in the first 10 min of leaching, the portion of REE presented in the fluorapatite lattice was leached and followed by leaching of the portions existing in the refractory minerals.

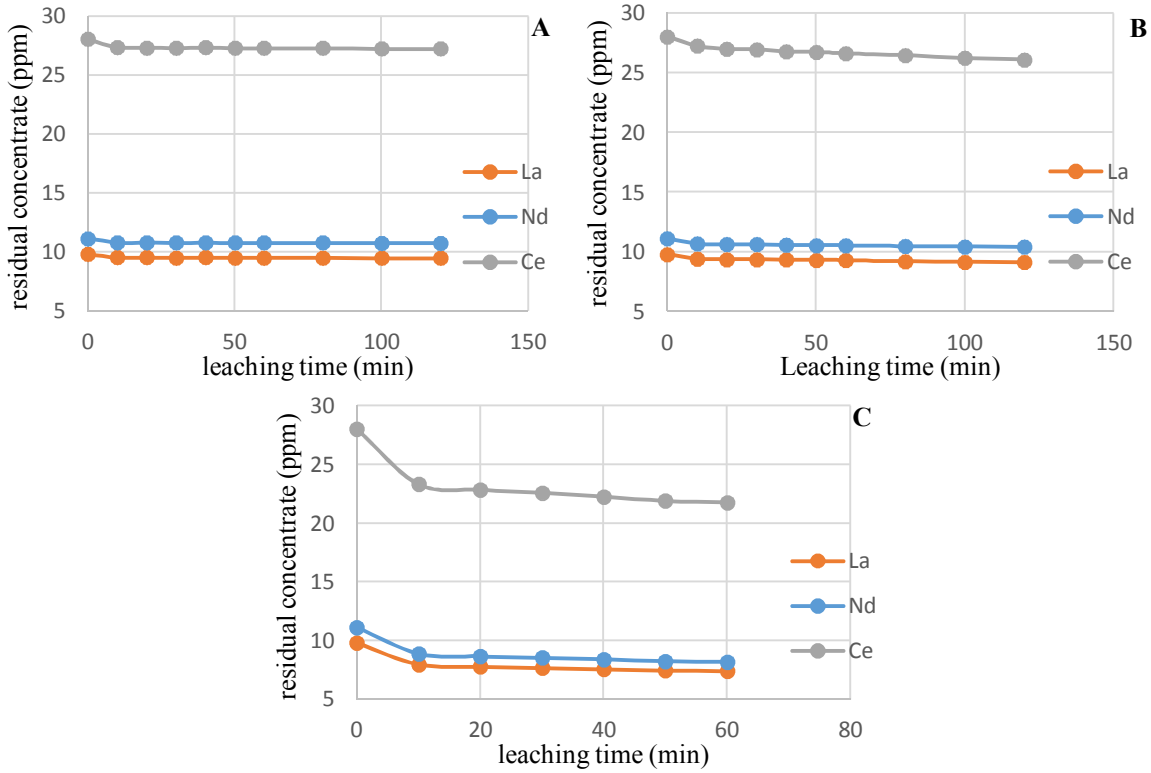


**Figure 9. Residual REE concentration (in leaching residue) curves against time from the leaching of phosphate concentrate at different temperatures: A) 60 ˚C, B) 70 ˚C, and C) 85 ˚C.**

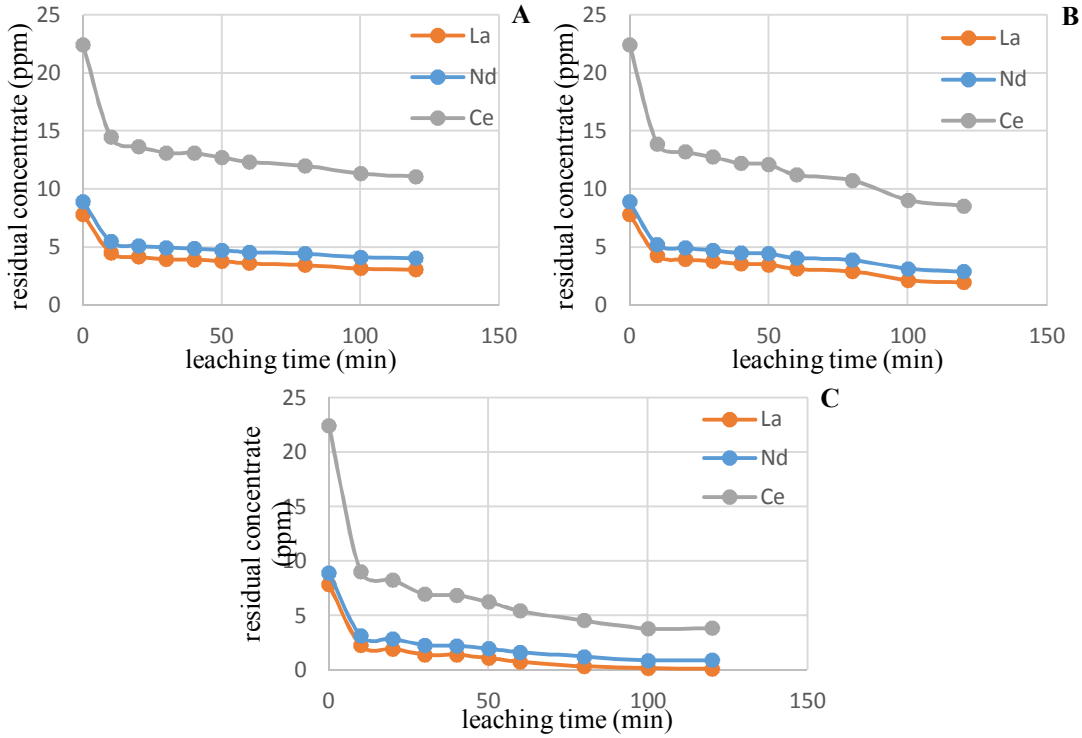


**Figure 10. Residual REE concentration (in leaching residue) curves against the time from leaching of the activated phosphate concentrate at different temperatures A) 60 ˚C, B) 70 ˚C, and C) 85 ˚C.**

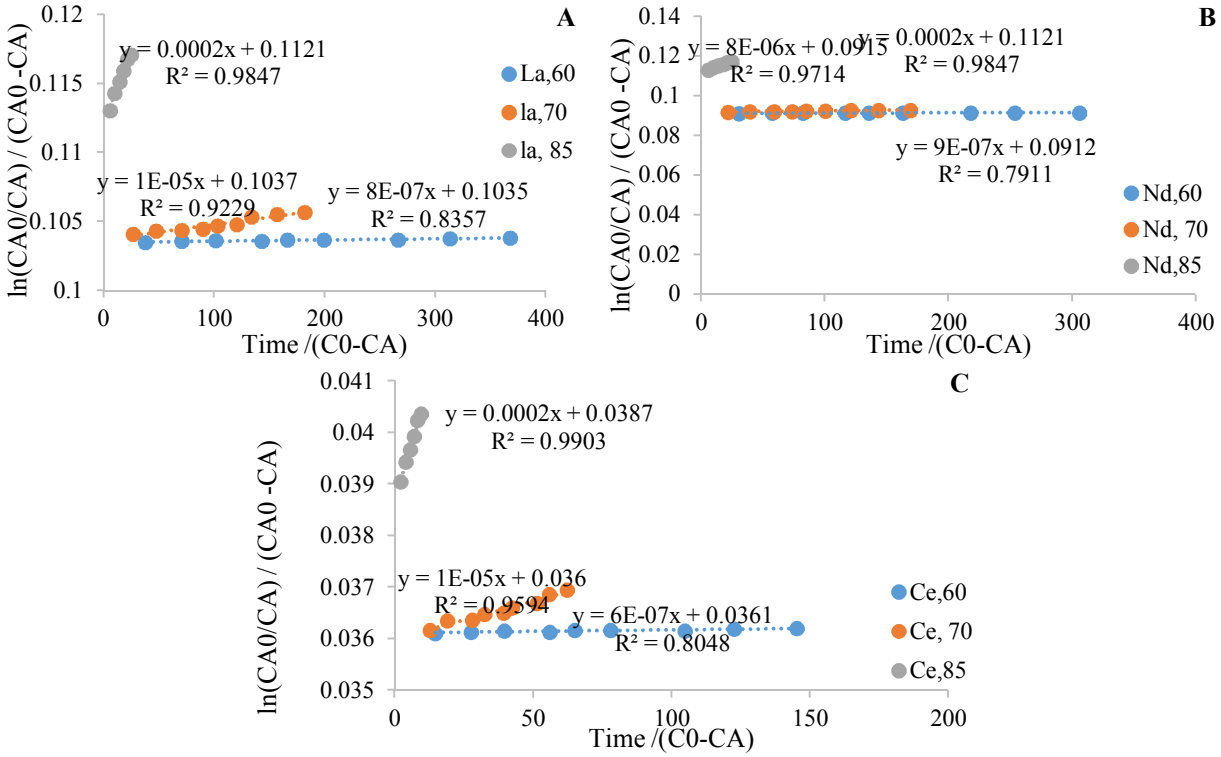


**Figure 11. Plots of $Ln(C_{A0}/C_A)/(C_{A0}-C_A)$ in terms of $t/(C_{A0}-C_A)$ for A) lanthanum, B) neodymium, and C) cerium leaching processes of the initial phosphate concentrate at 60, 70, and 85 °C.**

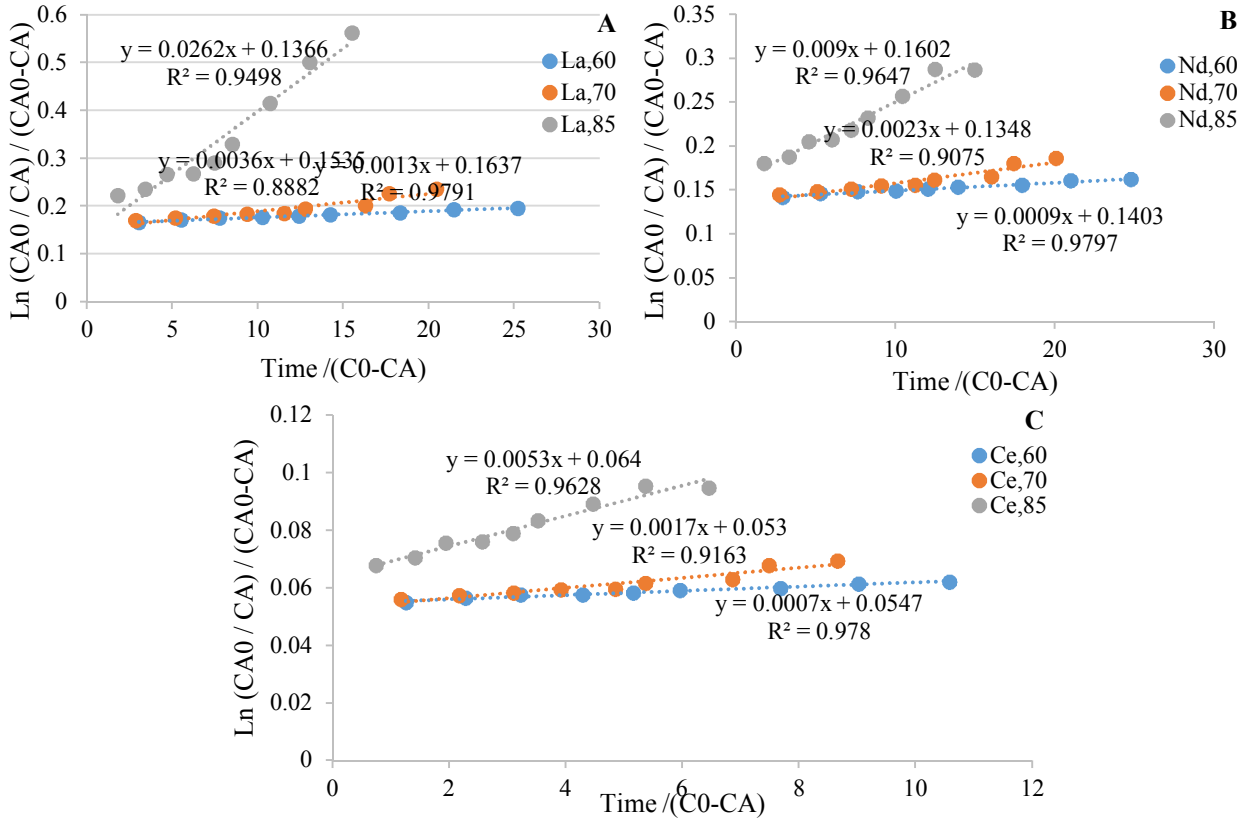


**Figure 12. Plots of $Ln(C_{A0}/C_A)/(C_{A0}-C_A)$ in terms of $t/(C_{A0}-C_A)$ for A) lanthanum, B) neodymium, and C) cerium leaching processes of the activated phosphate concentrate at 60, 70, and 85 °C.**

### 3.4.2. Apparent activation energy

The reaction rate constant was a function of temperature. After determining the appropriate kinetic model, the reaction rate constant was determined and used to draw the Arrhenius curve. The relationship between K and T is given by the Arrhenius relationship (Equation 13) [35]:

$$\ln K = \ln K + \frac{-E}{RT} \quad (13)$$

where $k_0$ and E are the frequency factor and the apparent activation energy, respectively. To calculate the activation energy, the Arrhenius curve of the leaching process was plotted using lnK values versus 1/T. Table 6 represents the leaching equations of the elements lanthanum, neodymium, and cerium for the activated and non-activated samples.

According to Table 7, the calculation of the apparent activation energy values showed that the first step of leaching for both the activated and non-activated samples had a high sensitivity to temperature, and its mechanism was a chemical control (more than 15 kJ/mol), and the second stage was a diffusion control (less than 15 kJ/mol) [36]. The apparent activation energy for the activated sample leaching process was significantly decreased compared to that of the non-activated sample. By activating the phosphate concentrate, the temperature had a less effect on the leaching, so the leaching of activated samples could be performed at a lower temperature than that of the non-activated ones.

**Table 6. The leaching equations of the elements lanthanum, neodymium, and cerium for the activated and non-activated samples.**

| Sample | Stage | Lanthanum | Neodymium | Cerium |
|---|---|---|---|---|
| **Non- activated sample** | First stage | $LnK = -25378x + 62.876$ | $LnK = -27826x + 69.549$ | $LnK = -27499x + 68.404$ |
| | Second stage | $LnK = -444.63x - 0.9459$ | $LnK = -422.52x - 1.1383$ | $LnK = -348.17x - 2.2881$ |
| **Activated samples** | First stage | $LnK = -14444x + 36.64$ | $LnK = -10992x + 25.987$ | $LnK = -9631.5x + 21.675$ |
| | Second stage | $LnK = -841.65 + 0.5526$ | $LnK = -682.08x + 0.0476$ | $LnK = -799.25x - 0.5431$ |

**Table 7. Apparent activation energy (kJ/mol) in the leaching of the elements lanthanum, neodymium, and cerium from the initial and activated phosphate concentrates.**

| Sample | Stage | Lanthanum | Neodymium | Cerium |
|---|---|---|---|---|
| **Non-activated sample** | First stage | 210.99 | 231.35 | 228.63 |
| | Second stage | 3.70 | 3.51 | 2.89 |
| **Activated sample** | First stage | 120.09 | 91.39 | 80.08 |
| | Second stage | 7 | 5.67 | 6.64 |

## 4. Conclusions

The XRD line profile analysis of the Williamson-Hall method was used for extracting the micro-structure characteristics of the mechanically activated phosphate concentrate. In order to extract the REEs in the normal leaching conditions, the mechanically activated samples were leached by a 32% nitric acid at 85 °C. The results of BET and laser diffraction analyses indicated that the agglomeration phenomenon began after 20 and 60 minutes of mechanical activation with 9.4 and 20 mm balls, respectively. A continuous increase of the specific surface area in the mechanical activation process using 9.4 mm balls showed that even after 90 minutes of mechanical activation, the pores were available for the nitrogen gas penetration. The high amorphization degree of the mechanically activated phosphate concentrate revealed the non-resistant nature of the phosphate concentrate. Therefore, the degree of amorphization of fluorapatite in the mechanically activated phosphate concentrate reached more than 85% after 60 minutes of high-intensity milling. Important information was obtained on the structural changes of the mechanically activated phosphate concentrate using the line profile analysis method. Using the Williamson-Hall method, the micro-strain and the volume-weighted crystallite size of fluorapatite were calculated in the initial phosphate concentrate sample (225 nm and 0.09%, respectively). After 20 minutes of mechanical activation with 9.4 and 20 mm balls, these values were changed to 90 nm, 0.66%, and 112.5 nm, 0.51%, respectively. In the leaching of the initial phosphate concentrate (not activated) at

85 °C for 120 minutes, the dissolution of Ce, La, and Nd was about 25.1%, 27.5%, and 24.3%, respectively. While an increase in the reactivity through the pre-treatment of mechanical activation using 9.4 and 20 mm balls for 20 and 60 minutes caused the dissolution of Ce, La, and Nd to reach their highest values (90.2, 98.9, and 88.4, 88.4, and 96.2, 87.2, respectively). Investigation of the kinetic models and calculation of the apparent activation energy showed that mechanical activation caused an increase in the REE leaching rate and a decrease in the activation energy. The results obtained showed that the leaching reaction had a high sensitivity to temperature, while by mechanical activation, the leaching was carried out at a lower temperature. Also it was concluded that the leaching of REEs from the activated and non-activated samples took place in two stages: in the first stage, the mechanism was a chemical-control (more than 15 kJ/mol), and in the second stage, it was a diffusion-control (less than 15 kJ/mol). Some of the potential concerns with the application of the mechanical activation process for the phosphate concentrates containing REE refractory minerals are techno-economic feasibility studies and using statistical methods for optimization of the overall process that require further investigations.

**Acknowledgments**
This research work was carried out with the financial support of the Tarbiat Modares University and IMIDRO in Iran. We thank them for their support.

**References**

[1]. Krishnamurthy, N. and Gupta, C.K. (2015). Extractive metallurgy of rare earths. CRC press.

[2]. https://minerals.usgs.gov.

[3]. Soltani, F., Abdollahy, M., Javad Koleini, S.M. and Moradkhani, D. (2017). Selection of an appropriate leaching method for light REEs from Esfordi flotation concentrate based on mineral characterization. Journal of the Southern African Institute of Mining and Metallurgy. 117 (5): 443-450.

[4]. Soltani, F., Abdollahy, M., Petersen, J., Ram, R., Becker, M., Koleini, S.J. and Moradkhani, D. (2018). Leaching and recovery of phosphate and rare earth elements from an iron-rich fluorapatite concentrate: Part I: Direct baking of the concentrate. Hydrometallurgy. 177: 66-78.

[5]. Baláž, P. (2000). Extractive metallurgy of activated minerals (Vol. 10). Elsevier.

[6]. Pourghahramani, P., Altin, E., Mallembakam, M.R., Peukert, W. and Forssberg, E. (2008). Microstructural characterization of hematite during wet and dry millings using Rietveld and XRD line profile analyses. Powder Technology. 186 (1): 9-21.

[7]. Baláž, P. (2003). Mechanical activation in hydrometallurgy. International Journal of Mineral Processing. 72 (1-4): 341-354.

[8]. Akhgar, B.N., Pazouki, M., Ranjbar, M., Hosseinnia, A. and Salarian, R. (2012). Application of Taguchi method for optimization of synthetic rutile nano powder preparation from ilmenite concentrate. Chemical Engineering Research and Design. 90 (2): 220-228.

[9]. Zhao, Z., Zhang, Y., Chen, X., Chen, A. and Huo, G. (2009). Effect of mechanical activation on the leaching kinetics of pyrrhotite. Hydrometallurgy. 99 (1-2): 105-108.

[10]. Basturkcu, H., Acarkan, N. and Gock, E. (2017). The role of mechanical activation on atmospheric leaching of a lateritic nickel ore. International Journal of Mineral Processing. 163:1-8.

[11]. Xu, Y., Jiang, T., Wen, J., Gao, H., Wang, J. and Xue, X. (2018). Leaching kinetics of mechanically activated boron concentrate in a NaOH solution. Hydrometallurgy.

[12]. Zhang, J.P. and Lincoln, F.J. (1994). The decomposition of monazite by mechanical milling with calcium oxide and calcium chloride. Journal of Alloys and Compounds. 205 (1-2): 69-75.

[13]. Kim, W., Bae, I., Chae, S. and Shin, H. (2009). Mechanochemical decomposition of monazite to assist the extraction of rare earth elements. Journal of Alloys and Compounds. 486 (1-2): 610-614.

[14]. Zhang, Q. and Saito, F. (1998). Non-thermal process for extracting rare earths from bastnaesite by means of mechanochemical treatment. Hydrometallurgy. 47 (2-3): 231-241.

[15]. Zhang, J. and Lincoln, F.J. (1993). The decomposition of $NdPO_4$ during mechanical milling. Journal of Alloys and Compounds. 200 (1-2): 151-156.

[16]. Tan, Q., Deng, C. and Li, J. (2016). Innovative application of mechanical activation for rare earth elements recovering: process optimization and mechanism exploration. Scientific Reports. 6: 19961.

[17]. Song, G., Yuan, W., Zhu, X., Wang, X., Zhang, C., Li, J. and Wang, J. (2017). Improvement in rare earth element recovery from waste trichromatic phosphors by mechanical activation. Journal of Cleaner Production. 151: 361-370.

[18]. Van Loy, S., Binnemans, K. and Van Gerven, T. (2017). Recycling of rare earths from lamp phosphor waste: Enhanced dissolution of LaPO4: Ce3+, Tb3+ by

mechanical activation. Journal of Cleaner Production. 156: 226-234.

[19]. Pourghahramani, P. and Forssberg, E. (2006). Microstructure characterization of mechanically activated hematite using XRD line broadening. International Journal of Mineral Processing. 79 (2): 106-119.

[20]. Pourghahramani, P. and Forssberg, E. (2007). The characterization of structural changes in hematite ground in a confined particle bed using Rietveld analysis. International Journal of Mineral Processing. 83 (1-2): 47-59.

[21]. Suryanarayana, C. and Norton, M.G. (1998). Practical aspects of X-ray diffraction. In X-Ray Diffraction (pp. 63-94). Springer, Boston, MA.

[22]. Lucks, I., Lamparter, P. and Mittemeijer, E.J. (2004). An evaluation of methods of diffraction-line broadening analysis applied to ball-milled molybdenum. Journal of Applied Crystallography. 37 (2): 300-311.

[23]. Baláž, P. (2008). High-energy milling. In Mechanochemistry in Nanoscience and Minerals Engineering (pp. 103-132). Springer, Berlin, Heidelberg.

[24]. Tahmasebi, R., Shamanian, M., Abbasi, M.H. and Panjepour, M. (2009). Effect of iron on mechanical activation and structural evolution of hematite–graphite mixture. Journal of Alloys and Compounds. 472 (1-2): 334-342.

[25]. Cullity, B.D. and Stock, S.R. (2014). Elements of X-ray Diffraction. Pearson Education.

[26]. Hu, H., Chen, Q., Yin, Z., Zhang, P. and Wang, G. (2004). Effect of grinding atmosphere on the leaching of mechanically activated pyrite and sphalerite. Hydrometallurgy. 72 (1-2): 79-86.

[27]. Lehmann, M.N., O'leary, S. and Dunn, J.G. (2000). An evaluation of pretreatments to increase gold recovery from a refractory ore containing arsenopyrite and pyrrhotite. Minerals Engineering. 13 (1): 1-18.

[28]. Zdujić, M., Jovalekić, Č., Karanović, L., Mitrić, M., Poleti, D. and Skala, D. (1998). Mechanochemical treatment of $\alpha$-$Fe_2O_3$ powder in air atmosphere. Materials Science and Engineering: A. 245 (1): 109-117.

[29]. Cullity, B.D., Stock, S.R. and Stock, S. (2001). Elements of X-ray Diffraction, 3rd edition, Prentice Hall. New Jersey.

[30]. Li, C., Liang, B. and Wang, H. (2008). Preparation of synthetic rutile by hydrochloric acid leaching of mechanically activated Panzhihua ilmenite. Hydrometallurgy. 91 (1-4): 121-129.

[31]. Tkáčová, K., Baláž, P., Mišura, B., Vigdergauz, V.E. and Chanturiya, V.A. (1993). Selective leaching of zinc from mechanically activated complex Cu Pb Zn concentrate. Hydrometallurgy. 33 (3): 291-300.

[32]. Ekinci, Z., Colak, S., Cakici, A. and Sarac, H. (1998). Leaching kinetics of sphalerite with pyrite in chlorine saturated water. Minerals Engineering. 11 (3): 279-283.

[33]. Breed, A.W. and Hansford, G.S. (1999). Studies on the mechanism and kinetics of bioleaching. Minerals Engineering. 12 (4): 383-392.

[34]. Levenspiel, O. (1999). Chemical reaction engineering. Industrial & Engineering Chemistry Research. 38 (11): 4140-4143.

[35]. Qiu, H., Lv, L., Pan, B.C., Zhang, Q.J., Zhang, W.M. and Zhang, Q.X. (2009). Critical review in adsorption kinetic models. Journal of Zhejiang University-Science A. 10 (5): 716-724.

[36]. Free, M.L. (2013). Hydrometallurgy: fundamentals and applications. John Wiley & Sons.

# فعال‌سازی مکانیکی کنسانتره فسفات برای افزایش کارآیی انحلال عناصر نادر خاکی از نقطه نظر سینتیکی

**هادی شادی نقده[۱]، محمود عبدالهی[۱*]، احمد خدادادی دربان[۱] و پرویز پورقهرمانی[۲]**

**۱- بخش مهندسی معدن، دانشگاه تربیت مدرس، ایران**

**۲- بخش مهندسی معدن، دانشگاه صنعتی سهند، ایران**

ارسال ۲۰۱۸/۱۱/۵، پذیرش ۲۰۱۹/۱/۲

* نویسنده مسئول مکاتبات: minmabd@modares.ac.ir

**چکیده:**

کنسانتره فسفات اسفوردی شامل فلوئورآپاتیت، مونازیت و زنوتیم به عنوان کانی‌های نادر خاکی است که عیار فلز نادر خاکی در آن ۱/۵ درصد است. کانی‌های مونازیت و زنوتیم مقاوم هستند و تجزیه آن‌ها تنها در دمای بالا ممکن است؛ بنابراین در این پژوهش فعال‌سازی مکانیکی برای این منظور استفاده شده است. پس از ۹۰ دقیقه فعال‌سازی مکانیکی، میزان آمورف شدگی اشعه ایکس و سطح مخصوص بیشینه BET به ترتیب به ۹۳/۴ درصد و ۸/۴ $m^2/g$ افزایش یافت. نمودار ویلیامسون- هال نشان داد که اندازه کریستالیت و کرنش شبکه‌ای به صورت تابعی از شدت آسیاکاری به ترتیب کاهش و افزایش یافت. برای نمونه فعال‌سازی شده مکانیکی به مدت ۹۰ دقیقه، اندازه کریستالیت بر اساس وزن حجمی برابر با ۶۴ nm و کرنش شبکه‌ای برابر با ۰/۹ درصد به دست آمد. کارآیی لیچینگ عناصر نادر خاکی با اسید نیتریک ۳۲ درصد و دمای ۸۵ درجه سانتی‌گراد، از ۲۵ درصد برای نمونه اولیه به حدود ۹۵ درصد برای نمونه فعال‌سازی شده افزایش یافت. ثابت‌های نرخ سینتیک مرحله اول در دمای ۶۰ درجه سانتی‌گراد برای La، Nd و Ce به ترتیب از $8\times10^{-7}$، $9\times10^{-7}$ و $6\times10^{-7}$ برای نمونه اولیه به $1.3\times10^{-3}$، $9\times10^{-4}$ و $7\times10^{-4}$ برای نمونه فعال‌سازی شده مکانیکی افزایش یافت. همچنین انرژی فعال‌سازی ظاهری La، Nd و Ce برای نمونه اولیه به ترتیب حدود ۲۱۰، ۲۳۱ و ۲۲۹ کیلوژول بر مول به دست آمد که برای نمونه فعال‌سازی شده مکانیکی به مدت ۲۰ دقیقه در اتمسفر آرگون به ترتیب به ۱۲۰، ۹۱ و ۸۰ کیلوژول بر مول کاهش یافت. نتایج، فعال‌سازی مکانیکی را به عنوان یک روش پیش‌فراوری مناسب (با هزینه کمتر و بازیابی بالاتر) برای انحلال عناصر نادر خاکی از کنسانتره فسفات حاوی کانی‌های مقاوم نادر خاکی پیشنهاد داد.

**کلمات کلیدی:** کنسانتره فسفات اسفوردی، عناصر نادر خاکی، فعال‌سازی مکانیکی، لیچینگ.